Plant Biology:

Oligomerization, membrane association and in vivo phosphorylation of sugarcane UDP-glucose pyrophosphorylase

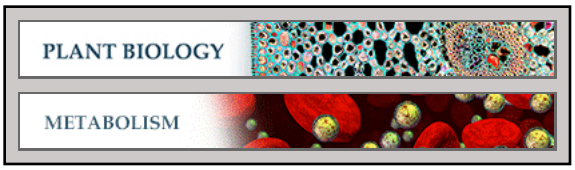

Jose Sergio M. Soares, Agustina Gentile, Valeria Scorsato, Aline da C. Lima, Eduardo Kiyota, Marcelo Leite dos Santos, Claudia V. Piattoni, Steven C. Huber, Ricardo Aparicio and Marcelo Menossi

J. Biol. Chem. published online October 15, 2014

JBC Papers in Press. Published on October 15, 2014 as Manuscript M114.590125
The latest version is at http://www.jbc.org/cgi/doi/10.1074/jbc.M114.590125

Oligomerization, membrane association and *in vivo* phosphorylation of sugarcane UDP-glucose pyrophosphorylase

Jose Sergio M. Soares[1], Agustina Gentile[1], Valeria Scorsato[2], Aline da C. Lima[2], Eduardo Kiyota[2], Marcelo Leite dos Santos[3], Claudia V. Piattoni[4], Steven C. Huber[5], Ricardo Aparicio[2] , Marcelo Menossi[1]

[1] *Departamento de Genética, Evolução e Bioagentes, Instituto de Biologia, Universidade Estadual de Campinas, C.P. 6109, Campinas, SP, Brazil*

[2]*Laboratório de Biologia Estrutural e Cristalografia, Instituto de Química, Universidade Estadual de Campinas, C.P. 6154, Campinas, SP, Brazil*

[3]*Centro de Ciências Exatas e Tecnologia, Núcleo de Química, Universidade Federal do Sergipe, C.P. 49500000, Itabaiana, SE, Brazil*

[4]*Instituto de Agrobiotecnologia del Litoral (UNL-CONICET), Universidad Nacional del Litoral, Ciudad Universitaria-Paraje El Pozo, CC242, S3000ZAA Santa Fe, Argentina*

[5]*Department of Agriculture Agricultural Research Service, and Department of Plant Biology, University of Illinois at Urbana-Champaign, Urbana, IL, 61801*

* Running title: *Factors affecting sugarcane UDP-glucose pyrophosphorylase activity*

To whom correspondence should be addressed: Marcelo Menossi, Departmento de Genética, Evolução e Bioagentes, Instituto de Biologia, Universidade Estadual de Campinas, Rua Monteiro Lobato, 255, Campinas, SP, Brazil, tel.: +55 (19) 3521-6236; +55 (19) 3521-6241; E-mail: menossi@lgf.ib.unicamp.br

Keywords: Redox regulation, kinetics, small-angle X-ray scattering (SAXS), gene expression, protein phosphorylation, sucrose.

Background: UDP-glucose pyrophosphorylase (UGPase) is a key enzyme in the biosynthesis of sucrose and the cell wall.
Results: UGPase was phosphorylated in and associated with the membrane *in vivo*. Redox modification modulated UGPase activity by changing its oligomeric state.
Conclusion: Phosphorylation, redox modification and oligomerization regulate UGPase.
Significance: Our data broaden the understanding of biomass biosynthesis in the bioenergy crop sugarcane.

ABSTRACT

Sugarcane is a monocot plant that accumulates sucrose to levels of up to 50% of dry weight in the stalk. The mechanisms that are involved in sucrose accumulation in sugarcane are not well understood, and little is known with regard to factors that control the extent of sucrose storage in the stalks. UDP-glucose pyrophosphorylase (UGPase; EC 2.7.7.9) is an enzyme that produces UDP-glucose, a key precursor for sucrose metabolism and cell wall biosynthesis. The objective of this work was to gain insights in the *ScUGPase-1* expression pattern and regulatory mechanisms that control protein activity. *ScUGPase-1* expression was negatively correlated with the sucrose content in the internodes during development, and only slight differences in the expression patterns were observed between two cultivars that differ in sucrose content. The intracellular

localization of *Sc*UGPase-1 indicated partial membrane association of this soluble protein in both the leaves and internodes. Using a phospho-specific antibody, we observed that *Sc*UGPase-1 was phosphorylated *in vivo* at the Ser419 site in the soluble and membrane fractions from the leaves but not from the internodes. The purified recombinant enzyme was kinetically characterized in the direction of UDP-glucose formation and the enzyme activity was affected by redox modification. Preincubation with H_2O_2 strongly inhibited this activity, which could be reversed by DTT. Small-angle X-ray scattering analysis indicated that the dimer interface is located at the C-terminus and provided the first structural model of the dimer of sugarcane UGPase in solution.

Most of the ethanol that is produced worldwide derives from plant juice containing sucrose from sugarcane in Brazil and starch from corn in the United States (1). The development of high-yielding sugarcane cultivars that are adapted to different conditions remains a major challenge for breeders (1). The current sugarcane cultivars are based on crosses between *Saccharum officinarum*, a domesticated sugar producing species and *Saccharum spontaneum*, a wild species. The *Saccharum* hybrid of these two species was backcrossed to *S. officinarum* to generate sugarcane with a complex genome that incorporates the higher sugar content of *S. officinarum* with the disease and stress resistance traits of *S. spontaneum* (2, 3).

Sucrose (α-D-glucopyranosyl-1,2-D-fructofuranose) is the world's most abundant disaccharide. Sucrose is produced primarily in leaf mesophyll cells and is then transported throughout the phloem. In many plant species, sucrose is exported to the apoplast prior to being loaded into the phloem. As a result, the concentration of sucrose in the leaf apoplast increases as photosynthesis occurs. Sugarcane is a C_4 plant that accumulates sucrose to levels of up to 50% of dry weight in the stalk (4).

UDP-glucose pyrophosphorylase (UGPase; EC 2.7.7.9) is an important enzyme for sucrose synthesis and cell wall formation and is essential for plant survival because a deficiency in UGPase activity causes male-sterility (5). This enzyme is responsible for the production of uridine diphosphate glucose (UDP-glucose) using glucose-1-phosphate (Glc-1-P) and uridine-5'-triphosphate (UTP) in source tissues. In sink tissues, the enzyme sucrose synthase can form UDP-glucose by cleaving sucrose, which is then utilized by UGPase to form glucose-1-phosphate. UDP-glucose is a substrate for cellulose and callose biosynthesis at the plasmalemma (6–10).

The mechanisms that are involved in sucrose accumulation in sugarcane are not well understood, and little is known with regard to the factors that control the extent of sucrose storage in the stalks and the production of cellulose, including the mechanisms that regulate UGPase activity. The UGPase activity in the UDP-glucose synthesis direction of the reaction occurs predominantly in photosynthetic tissues, directing carbon flux toward sucrose synthesis (10). Protein oligomerization is suppose to be a key regulatory mechanism controlling UGPase activity, possibly also controlling the entire pathway of sucrose synthesis (11). In addition, protein phosphorylation and the binding of 14-3-3 proteins could be other posttranslational modifications that are involved in regulating UGPase activity, subcellular localization and protein turnover. Barley UGPase binds to 14-3-3 proteins *in vivo* (12), and yeast UGPase phosphorylation does not affect its activity, but leads to a decreased glycogen content and an increased cell wall glucan content (13).

The objective of this work was to gain insight into the *ScUGPase-1* expression pattern and regulatory mechanisms of protein activity. Combining gene expression and immunoblotting analyses, *Sc*UGPase-1 was mainly distributed in the stems of sugarcane. There was a decrease in *ScUGPase-1* gene expression in the stems as the maturation progressed between two sugarcane cultivars differing in their ability to accumulate sucrose. *Sc*UGPase-1 was detected in the cytoplasm, in agreement with its role in sucrose synthesis. Interestingly, *Sc*UGPase-1 was also found to be associated with the plasma membrane, which could indicate a role in cellulose synthesis. In addition, using a phospho-specific antibody, we observed that *Sc*UGPase-1 was phosphorylated *in*

vivo at the Ser419 site in the soluble and membrane fractions of the leaves but not in those of the internodes. Finally, kinetics and small-angle X-ray scattering data provided evidence of a possible redox and oligomeric modulation of *Sc*UGPase-1 *in vitro*.

EXPERIMENTAL PROCEDURES

Plant Material - Sugarcane cultivars RB855156 (High Brix, HB) and RB935744 (Low Brix, LB) were grown in the field for 8 months at the Centro de Ciências Agrárias - UFSCAR (Araras - SP, Brazil). Samples of mature leaf (leaf +1) and the first, fifth and ninth internodes were collected from sugarcane cultivars with different agronomical traits concerning sucrose content. The tissues were sectioned, frozen in liquid nitrogen, and stored at - 80º C.

RNA isolation and quantitative PCR - RNA was isolated from a mature leaf and the first, fifth and ninth internodes using the RNeasy Plant Mini kit (Qiagen) following the manufacture's protocol. First strand cDNAs were synthesized using 2.5 µg of DNA-I treated RNA (500 ng/µL), oligo-dT_{17} primer and 10 mM dNTP mix. The RNA samples were denatured at 65º C for 10 min and placed on ice for 2 min, after which 5× First Strand Buffer, 0.1 M DTT and Superscript II RT enzyme (200 U/µL) were added (Life Technologies). The reaction was performed at 42º C for 50 min and at 70º C for 15 min in a thermocycler. Quantitative PCR (qPCR) was performed in the Applied Biosystems 7500 Real Time PCR System (Life Technologies). To each cDNA sample, SYBR Green PCR Master Mix (Life Technologies), 10 µM forward primer, 10 µM reverse primer and water were added. The C-terminal region of the coding sequence of the *ScUGPase-1* gene was used as a template to design the primers (Table 1). The reactions were incubated at 95º C for 10 min followed by 40 cycles at 95º C for 15 s and 60º C for 1 min as described by Varkonyi-Gasic and collaborators (14). The sugarcane polyubiquitin gene (CA179923) was used as a reference sample (15) using the primers that are described in Table 1. The reactions were conducted with three biological replicates, each in triplicate. The displayed qPCR result values are relative to those of a mature leaf in each cultivar. To calculate the fold change, we used the web-based qPCR system considering the primer reaction efficiencies (16).

Membrane extraction - Leaf and internode membranes were ground in an extraction buffer containing 20 mM Tris-HCl pH 8.8, 150 mM NaCl, 1 mM EDTA, 1 mM PMSF, 5 mM benzamidine and 4% (v/v) glycerol. The extract was spun at 6,000 × *g* for 15 min (4º C), and the resultant supernatant was further centrifuged at 100,000 × *g* for 2 h (4º C). The pellet was resuspended in 150 µL of resuspension buffer containing 10 mM Tris-HCl pH 7.3, 150 mM NaCl, 1 mM EDTA, 1 mM PMSF, 1 mM benzamidine, 1 mM $MgCl_2$, 1% (v/v) glycerol and 0.1% (v/v) Triton-X 100. The sample was clarified and centrifuged at 100,000 × *g* for 1 h (4º C). The total membrane protein in the supernatant was quantified by the Bradford method. The membrane protein was adjusted to 0.5 to 1.0 mg/mL.

Immunoblotting - For the immunoblot detection, the protein samples were separated on 7 or 10% polyacrylamide SDS gels and transferred to specific polyvinylidene fluoride fluorescence (PVDF) membranes (Millipore). The membranes were blocked in a 2% (v/v) fish gelatin solution in PBS buffer before being incubated with primary antibodies at a 1:1000 dilution in PBST buffer. The washes were performed in PBST, and an anti-rabbit Alexa Fluor 680-conjugated secondary antibody was used at a 1:10000 dilution in PBST. Barley anti-UGPase (anti-*Hv*UGPase) and phospho-specific (anti-pS419) primary antibodies used were polyclonal raised in rabbits. Immunoblots were generated using LI-COR Odyssey, and the signal was detected based on fluorescence.

Subcellular localization and confocal microscopy - The sequence that encodes *Sc*UGPase-1 was amplified by PCR using specific primers as described in Table 1 and cloned as an NdeI/BamHI fragment into a modified pRT104 vector (17), generating the construct pRT104::*Sc*UGPase-1-GFP. The cauliflower mosaic virus (CaMV) 35S promoter drove the expression of the fusion protein. The in-frame fusion of *GFP-ScUGPase-1* was confirmed by nucleotide sequence analysis. Particle bombardment was used to introduce the plasmid into onion inner epidermal cells with a biolistic helium particle accelerator system (Biomics)

under a pressure of 1000 psi. The plasmid was precipitated using tungsten M10 particles (Bio-Rad) in 50 µL of 2.5 mM $CaCl_2$ and 20 µL of 100 mM spermidine. The target distance between the stop screen and onion piece was set at 9 cm. After bombardment, the onion pieces were kept in darkness at 25º C for 24 h. Onion epidermal cells were examined in the National Institute of Science and Technology on Photonics Applied to Cell Biology (INFABIC) at the University of Campinas (UNICAMP) using a Zeiss LSM780-NLO confocal on an Axio Observer Z.1 microscope (Carl Zeiss). Single optical sections were scanned as resulting images for each transient expression.

Determination of hydrogen peroxide - The levels of hydrogen peroxide in the sugarcane internode and leaf extract were determined by the ferrous ammonium sulfate/xylenol orange method as previously described (18). The samples were measured at 560 nm absorbance and compared with standard samples of hydrogen peroxide. The measurements were conducted with three biological replicates.

Cloning, expression and protein purification - The pSPORT vector containing the sequence that encodes the *Sc*UGPase-1 protein was obtained from the SUCEST database, Sugarcane Assembled Sequence (SAS) number SCQGLR1062D04.g. The nucleotide sequence for full-length *Sc*UGPase-1 was amplified by PCR and cloned into the pENTR-D/TOPO vector, generating the construction pTOPO::*Sc*UGPase-1. The PCR was performed using specific primers that are described in Table 1. Taq AccuPrime DNA Polymerase (Invitrogen) was used to amplify the PCR products, which were then separated by gel electrophoresis and purified. The clones were created by the *in vivo* recombination using the gateway system of pTOPO::*Sc*UGPase-1 with the pET160-DEST destination vector (Life Technologies) in chemically competent *E. coli* TOP10 cells. The recombinant plasmid pET160::*Sc*UGPase-1 was transferred into *E. coli* DH5α cells and then sequenced. The recombinant plasmid pET160::*Sc*UGPase-1 was transformed into the competent *E. coli* BL21(DE3) strain by thermal shock for protein expression. The cells were grown in 2 mL of LB medium containing ampicillin (100 mg/mL) at 37º C, 250 rpm, for 16 h. The culture was used to inoculate 2 L of the same medium under the same culture conditions until the OD_{600} reached from 0.6 to 0.8. The expression of the recombinant *Sc*UGPase-1 was induced by the addition of isopropyl β-D-1-thiogalactopyranoside (IPTG) to a final concentration of 1 mM and incubated for 4 h. The culture was harvested by 10 min of centrifugation at 6,000 × *g*, 4º C, and stored for further use at -20º C. The bacterial pellet that was obtained from 2 L of liquid culture was suspended in 40 mL of binding buffer containing 50 mM sodium phosphate, 100 mM NaCl, and 5% glycerol, pH 7.4. The protease inhibitor PMSF (1 mM) was added, along with lysozyme (1 mg/mL). The cells were lysed by sonication on ice in an ultrasonic cell disruptor (Cole–Parmer Instrument, Chicago, IL, USA). The lysate obtained was centrifuged at 27,000 × *g* for 30 min at 4º C. The supernatant containing the soluble cellular material (total volume of 80 mL) was used for purification using immobilized metal ion affinity chromatography (IMAC). A column containing 1.5 mL of Ni–NTA agarose resin (Qiagen) was equilibrated with 10 column volumes (CV) of binding buffer. The supernatant was loaded onto the column by gravity. The column was washed with 10 CV of wash buffer containing 50 mM sodium phosphate, 100 mM NaCl, 5% glycerol, and 10 mM imidazole, pH 7.3. The recombinant 6× his-tagged *Sc*UGPase-1 was eluted with binding buffer containing increasing imidazole concentration (10, 20, 50, 100 and 200 mM). Fractions containing the full length 6× his-tagged *Sc*UGPase-1 protein were pooled and analyzed by 12% SDS-PAGE to determine the molecular mass and purity of the protein. The total protein concentration was determined by A_{280} quantification. At this point, one fraction of the purified protein was collected for gel filtration chromatography, while the other fraction was submitted to 6× his-tag cleavage. Following IMAC of the 6× his-tagged *Sc*UGPase-1, the purified protein was pooled, and recombinant tobacco etch virus (rTEV) 6× his-tagged protease was added in a 1:10 rTEV: protein ratio. Following the incubation, the protein sample was loaded onto a gravity flow Ni-NTA column pre-equilibrated in buffer containing 50 mM sodium phosphate, and 100 mM NaCl, pH 7.4, for a second affinity chromatography to separate the 6× his-tag from *Sc*UGPase-1. The flow-through

containing the protein was collected, dialyzed against buffer containing 50 mM sodium phosphate pH 7.4, 100 mM NaCl, and 5% glycerol and finally concentrated to 1-10 mg/mL using the Vivaspin 10 kDa MWCO Ultrafiltration spin column (GE Healthcare).

Enzyme activity and kinetic characterization - The activity of *Sc*UGPase-1 was assayed in the direction of synthesis of UDP-glucose as previously described (19). The assay was performed at 25º C. The reaction was conducted in a buffer containing 20 mM MOPS, pH 7.5, 1 mM DTT, 5 mM $MgCl_2$, 1.5 mM Glc-1-P, 1 mM UTP, 0.015 U/µL pyrophosphatase, 0.2 mg/mL BSA, and the purified protein at a 1:100000 dilution in a total volume of 60 µL. Malachite-green color reagent was added to finish the reaction. The samples were read at 650 nm with a spectrophotometer. The kinetic data were plotted as specific activity ($\mu mol \cdot min^{-1} \cdot mg^{-1}$) *versus* substrate concentration. Kinetic constants were acquired by fitting the data to the Hill equation with a non-linear least-squares formula using the program Origin version 7.0. Hill plots were used to calculate Hill coefficient and the kinetic constants that correspond to the maximal velocity (V_{max}), catalytic constant (k_{cat}), as well as the concentration of the substrate that leads to the half-maximal velocity (K_m). The kinetic constants are means of at least three independent set of data that were reproducible within ± 10%.

Redox modification - For the oxidation assay, the purified *Sc*UGPase-1 was incubated in a buffer containing 20 mM MOPS pH 7.5 at 25º C for 30 min in the presence of different concentrations of hydrogen peroxide (H_2O_2). After incubation, aliquots were withdrawn and assayed for *Sc*UGPase-1 activity. For the reduction assay, the oxidized enzyme was incubated in the same buffer as above in the presence of different concentrations of DTT. After 30 min of incubation, aliquots were withdrawn and assayed for *Sc*UGPase-1 activity. The reactions were performed as previously described (19).

Gel filtration - The 6× his-tagged *Sc*UGPase-1 was incubated in a buffer containing 20 mM MOPS, pH 7.5, 150 mM NaCl, 1mM EDTA, and 1 mM hydrogen peroxide (H_2O_2) for 30 min, and 200 µL of the oxidized *Sc*UGPase-1 was applied to a Superdex 200 10/300 GL column (GE Healthcare) on an AKTA FPLC system (GE Healthcare). A 20 mM MOPS, pH 7.5, 150 mM NaCl, and 1 mM EDTA mixture was used as the elution buffer. The flow rate was 0.5 mL min^{-1}. Fractions of 1 mL were collected. The fractions corresponding to a dimer of the 6× his-tagged *Sc*UGPase-1 were pooled and concentrated to 0.684 mg/mL using an Amicon Ultra-4 10kDa MWCO centrifugal filter (Millipore).

SAXS data collection and reduction - The SAXS data for the monomeric form of *Sc*UGPase-1 in buffer containing 50 mM sodium phosphate pH 7.2, 5% glycerol, and 100 mM NaCl, were collected at the wavelength λ = 1.49 Å using a MAR CCD 165 detector on the SAXS-2 beamline of the Brazilian National Synchrotron Light Laboratory (LNLS/Brazil) (20) with a sample-to-detector distance of 890.26 mm over a range of $0.0159 < q < 0.3751$ $Å^{-1}$ ($q=4\pi\sin\theta/\lambda$, where 2θ is the scattering angle). The scattering patterns were measured with a 300 s exposure time at 12º C, for samples with concentrations in the range 1.0 to 10.5 mg/mL. CCD Dark current and natural background correction were performed on the raw 2D images as appropriate. A subsequent data collection was performed at LNLS on the beamline SAXS-1 with a wavelength of 1.55 Å using a Dectris-Pilatus (300K, 84 mm × 107 mm) 2D detector. On this occasion, samples of a construct of *Sc*UGPase-1 with an additional N-terminus of 32 amino acid residues, including six histidines (MHHHHHHGAGGCCPGCCGGGENLYFQGII TSL) in a buffer containing 20 mM MOPS, pH 7.5, 150 mM NaCl, and 1 mM EDTA were analyzed at concentrations of 0.64, 2.09 and 2.32 mg/mL, the first of which was later found to correspond to a protein dimer in solution. X-ray scattering data were collected at 17º C and the sample-to-detector distance was 1603.43 mm, covering a momentum transfer interval of $0.0067 < q < 0.2780$ $Å^{-1}$. The protein samples that were initially kept on ice, were centrifuged for ~ 5 min at 14,100 × *g* and room temperature, prior to injection in the sample holder. To reduce potential radiation damage, for each sample, successive frames were recorded with exposure times ranging from 3 s to 400 s. The corresponding buffer solutions were measured for 100 s. For the data

that were collected at the beamline SAXS-1, absolute calibration of the scattering intensity was performed using water as a secondary standard (21, 22). Correction by sample attenuation, normalization of the collected images to the intensity of the transmitted beam, buffer scattering subtraction and radial integration were performed with FIT2 (23).

SAXS profile analysis and overall parameters - The scattering-intensity profiles were analyzed with ATSAS 2.5.1.1 (24) running under Slackware Linux (http://www.slackware.com). The zero-angle scattering intensity, I(0), and the radius of gyration, R_g, were calculated from data at very low q values ($qR_g \lesssim 1.3$) using the Guinier approximation (25) $I(q) = I(0)\exp(-q^2R_g^2/3)$. The pair-distance distribution function, P(r), was calculated by the indirect Fourier transform method using GNOM (26), from which additional estimates for R_g and I(0) were also obtained. The Kratky plot (27–29) was used to assess the conformational state of the protein in solution. The molecular masses were estimated by the excluded particle volume that was calculated from the scattering curves using GNOM and DATPOROD (24) as well as by the procedure that was described by Fischer and colleagues (30). These methods are independent of sample concentration, which was not determined with enough accuracy in either case, the monomer or dimer (6× his-tag construct).

Ab initio envelope reconstruction - *Ab initio* low-resolution envelopes for the scattering particles in solution were determined from the scattering curves as follows. The curve corresponding to the *Sc*UGPase-1 monomer included scattering up to q=0.3751 $Å^{-1}$, which prompted us to use GASBOR (31) for shape recovery, a software which implements a simulated annealing algorithm based on a chain-like assembly of dummy residues that consider the internal structure of the protein. The GASBOR models were recovered from the scattering curve using default parameters and a total number of residues equal to 476. For the protein dimer, whose final curve was limited to the lower q_{max}=0.2 $Å^{-1}$, DAMMIF (32) was used instead. For better results, the annealing parameters were initially fine-tuned by running DAMMIF in the interactive mode. Convergence was assured by using prolate particle anisometry, as indicated by the asymmetric profile of the dimer P(r), along with the expected point-group P2 symmetry as inferred from available homolog crystal structures. The looseness penalty was adjusted to a value of 0.2 to reject unlike models, and an atomic radius of 1.5 was employed, leading to a higher number of beads and finer details on the volume surface. In both cases, to verify the reliability and reproducibility of the adopted procedure, 40 models were obtained in independent runs, and were subsequently analyzed using DAMAVER (33). The cross correlation table based on the normalized spatial discrepancy (NSD) confirmed the stability and reliability of the *ab initio* shape determination. From the 40 models that were initially obtained for the monomer, 5 outliers were automatically discharged. The NSD for the remaining 35 models was 0.96 ± 0.04, indicating a very narrow spatial distribution of the GASBOR models. The same procedure led to an NSD=0.55 ± 0.12 for the dimer after the exclusion of a single outlier, which assures a highly significant similarity between the solutions that were found by DAMMIF. In the dimer case, DAMAVER version 3.2 was used to correctly handle the model symmetry. To maintain the original features of the most typical GASBOR model, the model with the lowest average NSD compared to the others was reported. For the dimer, the final model that was obtained with DAMFILT after averaging is presented.

Molecular modeling - Despite numerous attempts the crystallization of *Sc*UGPase-1 was not successful. Thus, the envelopes that were recovered from the SAXS experiments were interpreted based on a computational model that was built using the I-TASSER server (34). An approach that combines threading and the SAXS profile for fold-recognition as implemented in the SAXSTER server (35) was also used, with no significant improvement compared to the previous approach, most probably due to the globular protein shape and the high sequence identity of the available homolog models. Therefore, the I-TASSER model with the highest confidence score (C-score=1.14), was chosen to represent the three-dimensional atomic structure of the *Sc*UGPase-1

monomer. To interpret the SAXS envelope for the *Sc*UGPase-1 dimer in solution, a template was selected based on a large-scale assessment of possible dimers that were obtained from available homolog crystal structures by applying crystallographic symmetry operators. For each possible dimer, a theoretical scattering curve was calculated and fitted to the *Sc*UGPase-1 experimental data with CRYSOL (36). The best agreement was obtained for a dimer that was constructed by applying crystal symmetry operations to the contents of the asymmetric unit that was reported for the homolog UGPase from *Arabidopsis thaliana* (PDB ID: 1Z90) (37). This arrangement was observed in various other homolog crystal structures, as discussed below. The final model for the *Sc*UGPase-1 dimer was obtained by individually superposing the *Sc*UGPase-1 monomer onto chains A and B of the referred structure and combining the resulting monomer chains. Throughout the processing, C shell scripts were used to automate computational jobs. Superpositions were performed with SUPCOMB (38). Data plotting was conducted with GNUPLOT (http://www.gnuplot.info) and model visualization and graphical analyses were performed with RASMOL (39) and PyMOL (The PyMOL Molecular Graphics System, version 1.4.1, Schrödinger, LCC).

RESULTS

ScUGPase-1 expression in sugarcane - In plants, *UGPase* genes are expressed in all tissues, including the roots, tubers, leaves, stems and young seeds (40). To evaluate the expression of the *ScUGPase-1* gene (GenBank accession number KF278717), we investigated its expression in the internode and mature leaf tissues of sugarcane cultivars that differ in their ability to accumulate sugar (Fig. 1). In sugarcane, the youngest internode (number 1) is the one at the top of the plant, close to the leaves, while the oldest internodes with a higher sugar content are those closest to the ground. *ScUGPase-1* expression decreased with internode maturation. The gene was also expressed in the leaves, although at lower levels, even when compared to mature internode number 9.

Protein localization and phosphorylation - UDP-glucose is a precursor for cell wall biosynthesis in photosynthetic tissues (8), where *Sc*UGPase-1 exists predominantly as a soluble cytosolic protein (41). In barley, high UGPase activities were found in the membrane fraction (42). To evaluate the *Sc*UGPase-1 expression in the sugarcane internode and leaf, the soluble and membrane fractions were extracted and analyzed by immunoblotting using the anti-*Hv*UGPase antibody. *In vivo*, *Sc*UGPase-1 also cross-reacted with the anti-*Hv*UGPase antibody and was present in the soluble and membrane fractions of the internode (Fig. 2A) and leaf (Fig. 2B) tissue. Interestingly, in Fig. 2B, we noticed the presence of a ~100 kDa band in both of the leaf tissue fractions. The size is consistent with a putative homodimer of the protein *Sc*UGPase-1. Despite this unexpected result, several authors have observed that proteins with different oligomeric forms present some degree of resistance to the conditions used in the SDS-PAGE (43–46). Strategically located disulfide bonds, salt bridges and hydrophobic residues at the surface of the proteins have been suggested as potential characteristics that could explain the resistance of some proteins to reducing agents (46). In addition, posttranslational modification may regulate the protein activity. The amino acid sequence of *Sc*UGPase-1 is strongly conserved among other plant UGPases (Fig. 3) and contains a serine at position 419 that is predicted to be a phosphorylation site and a 14-3-3 binding site (12). To evaluate *Sc*UGPase-1 in relation to its phosphorylation status *in vivo*, we once again extracted the soluble and membrane fractions from sugarcane internode and leaf and immunoblotted the crude extract using the anti-pS419 antibody. *Sc*UGPase-1 phosphorylation was not detected in the internode (Fig. 4A), while in the soluble and membrane fractions from the leaves, a clear phosphorylation signal was observed (Fig. 4B). To complement the results in Fig. 2, a GFP-*Sc*UGPase-1 fusion protein was transiently expressed in the onion epidermis, indicating not only cytosolic localization, but also an association with the cell membrane (Fig. 5), these findings are, consistent with the fractionation and immunoblotting analyses.

Levels of hydrogen peroxide in the internode and leaves - Fig. 2B indicates the presence of a putative *Sc*UGPase-1 dimer in

sugarcane leaves. In addition, oxidizing agents regulate the quaternary state of UGPase (47). Therefore, we evaluated the range of levels of H_2O_2 internode and leaf tissues of sugarcane. In the internodes, the presence of H_2O_2 was almost undetectable, while in the leaves, we observed a range between 1 µmol/g FW and 2.5 µmol/g FW, which is equivalent to 20 mM and 50 mM H_2O_2, respectively (data not shown). These values are compatible with the levels of H_2O_2 in field grown plants in a study that suggested a normal range between 1 and 5 µmol/g FW (48). These results indicating higher levels of H_2O_2 in sugarcane leaves corroborate the notion that H_2O_2 may influence the oligomeric state of *Sc*UGPase-1 *in vivo*.

Cloning, expression and protein purification - To produce the recombinant *Sc*UGPase-1, we cloned the entire coding sequence into the pET160-DEST vector. The protein was expressed in BL21(DE3) cells and purified by affinity chromatography onto a Ni-NTA agarose resin. The 6× his-tagged *Sc*UGPase-1 was obtained with high purity as determined by SDS-PAGE (Fig. 6, lane 1). We also produced the recombinant protein without the his-tag by treating the 6× his-tagged *Sc*UGPase-1 with rTEV protease. After a new IMAC purification to remove the rTEV and the his-tag, the cleavage protein yielded a polypeptide with a molecular mass of approximately 52 kDa as determined by SDS-PAGE (Fig. 6, lane 2), in which two elution fractions corresponding to the oligomers and the dimer of 6× his-tagged *Sc*UGPase-1 for the small-angle X-ray scattering (SAXS) experiment were collected (see below). Then, the 6× his-tagged *Sc*UGPase-1 was also submitted to affinity chromatography on an Ni-NTA agarose resin followed by protease cleavage. After cleavage with the rTEV protease, the purification yielded a protein with a high level of purity and a molecular mass of approximately 52 kDa as determined by SDS-PAGE (Fig. 2).

Characterization of ScUGPase-1 activity - To calculate the kinetic parameters of the recombinant *Sc*UGPase-1, we evaluated the enzyme activity at different concentrations of substrates in the direction of UDP-Glc synthesis. Fig. 7 presents the hyperbolic saturation curves for UTP (Fig. 7A), Glc-1-P (Fig. 7B) and Mg^{2+} (Fig. 7C) that were used to calculate the kinetic parameters (Table 2). The K_m values for Glc-1-P and UTP were 0.20 mM and 0.16 mM, respectively. The V_{max} for UDP-glucose synthesis was 2,151 ± 67 µmol·min^{-1}·mg^{-1}, corresponding to a k_{cat} number of 1.8×10^8 s^{-1}. The *Sc*UGPase-1 activity is approximately 6 fold higher than that determined for the recombinant UGPases from *Arabidopsis thaliana*. However, the substrate affinities were similar to those found for the recombinant UGPase1 and UGPase2 from *Arabidopsis* (49).

Redox modulation - According to Martinez *et al*., 2011, UGPase activity from *Entamoeba histolytica* is regulated by redox mechanisms affecting the activity of the enzyme involving oxidative and reducing agents that are generally found *in vivo*. To evaluate the effects of redox modification on *Sc*UGPase-1 activity the recombinant protein was incubated with H_2O_2 and DTT. *Sc*UGPase-1 activity was reduced by almost 80% when incubated with 20 mM H_2O_2 (Fig. 8A) and was restored after incubation with DTT (Fig. 8B). The reversible effect on the enzyme activity indicates a probable regulation of the protein *in vivo* according to the redox status of the cell. In addition, to evaluate the effects of redox modification on the oligomeric state of the protein, gel filtration chromatography using a Superdex 200 10/300 GL column was performed. The oxidation also affected the quaternary structure of the protein. In fact, the recombinant oxidized 6× his-tagged *Sc*UGPase-1 eluted as dimers and oligomers (data not shown). For a deeper structural characterization, the fraction that was recovered as a dimer was used for a small-angle X-ray scattering (SAXS) experiment.

SAXS overall parameters and molecular envelopes - To obtain a structural model of *Sc*UGPase-1 in solution, we performed a small-angle X-ray scattering experiment. The final SAXS scattering curves that were obtained from two different constructs of *Sc*UGPase-1, referred to as monomer and dimer, the latter including a 6× his-tag N-terminus, are shown in Fig. 9A and B, respectively. The linearity of Guinier plots was used to indicate data quality and monodispersity. The contribution of small amounts of potential higher-order oligomers that were detected at very low q values was reduced by carefully limiting the

lowest q value in the scattering curves. For the monomer, the best results were obtained for the sample at a protein concentration of 10.5 mg/mL.

In the case of the dimer curve (Fig. 9B), a cut-off at higher angles was also applied by discharging extremely noisy data that were observed for $q > 0.2$ Å^{-1}, which were a result of the low sample concentration (0.64 mg/mL). The analysis of the samples of this construct that were prepared at higher concentrations indicated the presence of higher-order oligomers, preventing further data processing. A sequential series of scattering patterns with increasing exposure time was measured for the lowest concentration sample. Visible changes in the sequential scattering profiles were clearly correlated with the cumulative exposure time. Thus, to prevent possible artifacts decurrent from radiation damage, only the first curve (Fig. 9B) was used for subsequent analyses.

The Kratky plots (Fig. 9C) exhibited a maximum that is typical for compact, correctly enovelated globular proteins. The R_g estimates that were calculated from the linear regression in the Guinier region (Fig. 8A and B, inset) were 27.5 Å and 50.8 Å for the monomer and dimer samples, respectively.

More accurate values for R_g were obtained from the indirect Fourier transform that was performed with GNOM (26), which considers the full-range scattering curve to calculate the distance distribution functions that were shown in Fig. 9D. For the monomer, the maximum intramolecular distance was 85.0 Å, resulting in an R_g that was also equal to 27.5 Å. The corresponding excluded volume that was calculated with AUTOPOROD (24) was V_p = 85.9 nm^3, allowing to estimate the molecular mass of the protein in solution as 53.0 kDa, in excellent agreement with the value of 56.1 kDa that was calculated by the method that was described in Fischer *et al.*, (30), with the linear and angular coefficients that were determined for $q_{max} = 0.30$ Å^{-1}. These results are consistent with the presence of a *Sc*UGPase-1 monomer in solution, whose molecular weight as calculated from the amino acid sequence was MW=53.3 kDa.

The dimer P(r) has a maximum intramolecular distance of 152.7 Å, from which R_g was estimated at 45.7 Å, in good agreement (within error) with the value that was predicted from the Guinier analysis. The two maxima that were noted in the P(r) profile are typical for protein dimers in solution. The molecular mass of the scattering particle in solution resulted was 105.4 kDa, as calculated from an excluded volume of V_p = 170.7 nm^3 (24), and 114.4 kDa (for q_{max} = 0.15) (30). In addition, despite the inherent limitations of this technique, the molecular mass estimated is consistent with the expected value MW=2×55.6=111.2 kDa, which was calculated taking into account the 6× his-tag in the construct, which unequivocally indicates the presence of an *Sc*UGPase-1 dimer in solution.

The SAXS envelopes that were recovered from the scattering curves are shown in Fig. 10. The excellent fitting of the theoretical curves that were computed with CRYSOL with the *Sc*UGPase-1 monomer and dimer models that were obtained by computational methods (Fig. 9A and B, respectively) can be visually confirmed by the corresponding superpositions that are shown in Fig. 10.

DISCUSSION

In plants, *UGPase* genes are expressed in all tissues, including the roots, tubers, leaves, stems and young seeds (40). In banana, *UGPase* genes are up-regulated by ethylene (50), whereas *UGPase* genes are up-regulated by phosphate deficiency, light exposure and sucrose supplementation in potato (51, 52). In this study, we evaluated the correlation between the sucrose content and *ScUGPase-1* gene expression in the sugarcane cultivars RB855156 (with a higher sucrose content) and RB935744 (with a lower sucrose content), but the *ScUGPase-1* profiles were very similar in these cultivars. Sucrose accumulation is under a complex regulatory network, and *ScUGPase-1* most likely acts in concert with the expression of genes encoding other key enzymes that are involved in sucrose production, such as sucrose synthase, sucrose phosphate synthase and invertases (53, 54). Interestingly, in both of the cultivars, *ScUGPase-1* expression in the internodes was modulated during

the maturation process, with higher expression during the early stages of internode maturation, suggesting a possible role of *Sc*UGPase-1 in cell wall biosynthesis. In addition, the elongation of sugarcane internodes is followed by increasing sucrose concentration (53). The accumulation of UGPase products decreases the protein activity (10). In addition, there is evidence of regulation at the gene expression level (eventually having affecting on UGPase protein content/activity), suggesting tight posttranscriptional/translation control (55, 56).

The *Sc*UGPase-1 localization and phosphorylation state were also studied. *Sc*UGPase-1 is predominantly found in the cytoplasm (10), but rice and tobacco cells also contain high UGPase activity in microsomes (57), and barley presents UGPase in plasmalemma membranes (42). Our results, which are a combination of the transient expression of GFP-*Sc*UGPase-1 in the onion epidermis and plant protein extract immunoblots, indicated that the protein is located in both the soluble and membrane fractions. The presence of a membrane-bound form of *Sc*UGPase-1 producing UDP-glucose would facilitate an efficient transfer of the glucose molecule in channeling carbon into cell wall glucans. In sink tissues, UDP-glucose is mainly derived from UGPase and sucrose synthase reactions (58). Sucrose synthase (SuSy) content is low in mature leaves but is active and prominent in sink tissues, breaking down sucrose into UDP-glucose and fructose. Phosphorylation modifies SuSy activity (promoting UDP-Glc production) and protein localization (favoring membrane dissociation) (59). We speculate that both of the enzymes work in concert to produce UDP-Glc.

Protein phosphorylation has also been described as a regulatory mechanism in UGPases from *Arabidopsis thaliana* (49) and *Saccharomyces cerevisiae* (60). *Sc*UGPase-1 contains the sequence RFKS^{419}IPSI, which is a crucial motif for the phosphorylation and binding of 14-3-3 proteins (61), including a characteristic phosphoserine residue at position 419. Interestingly, *Sc*UGPase-1 was phosphorylated *in vivo* in the cytoplasm and membranes from leaf tissues but not in those from internodes. In source tissues, SPS is considered the major enzyme that is involved in the conversion of photoassimilate to sucrose and uses the UDP-Glc that is provided by UGPase. SPS activity is regulated by covalent modification via phosphorylation/dephosphorylation (61) and via allosteric effectors (62). Sucrose accumulation increases under light, while dark conditions lead to starch degradation (56). During the day, SPS is active, during the night or when the rate of sucrose synthesis exceeds the capacity of the leaf to export or store sucrose, SPS is phosphorylated and binds to 14-3-3, which leads to the inhibition of SPS activity and sucrose synthesis (61). Based on our results, *Sc*UGPase-1 was phosphorylated only in leaf tissues. The lack of phosphorylation in the plasmalemma from internode tissues suggests that, in sink tissues, the *Sc*UGPase-1 reaction is linked to the SuSy reaction to provide substrate for cellulose biosynthesis. This assumption has already been addressed by Kleczkowski *et al*., 2010, who suggested that UDP-glucose comes from the UGPase reaction, as *Arabidopsis sus* mutants (63) presented the same phenotype as that of the wild-type with respect to growth and development. In addition, in a recent study, UGPase was demonstrated to be involved in plant height growth and biomass accumulation (9). We speculate that in source tissues, *Sc*UGPase-1 activity is regulated by the phosphorylation of a serine at the 14-3-3 binding site. It is possible that this regulation acts in coordination with SPS, but further study is required to establish the effect of *Sc*UGPase-1 phosphorylation and to identify its physiological significance.

Further characterization of the *Sc*UGPase-1 enzymatic activity and its regulatory mechanisms demonstrated that the kinetic properties of the recombinant enzyme are similar to those that have been previously reported for other UGPases, even when the enzymatic activity was approximately 6 fold higher than that described for the *Arabidopsis* recombinant enzymes. Furthermore, when the catalytic efficiency is estimated by the ratio k_{cat}/K_m ($s^{-1}\cdot mM^{-1}$), it is clear that the recombinant *Sc*UGPase-1 is approximately 2 times more efficient than are recombinant *At*UGPases (49).

The activity of *Sc*UGPase-1 was also modulated by redox compounds. The redox assay showed that the oxidized agent H_2O_2 inactivated *Sc*UGPase-1, and this inhibition was completely

reversed by the addition of the reducing agent DTT. This result agrees with the previous report demonstrating that the activity of UGPase from *E. histolytica* is modulated by redox mechanisms (47). Reactive oxygen species (ROS), which include hydrogen peroxide (H_2O_2), play crucial roles in modulating many physiologic and pathologic processes *in vivo*. Abiotic stresses, such as excess light, drought, and salt stress, enhance the production of reactive oxygen species, and proteomics analysis demonstrated that UGPase activity is reduced by salt stress (64). In addition, higher photosynthetic activity induces both the generation of ROS and the accumulation of soluble sugars (65). In agreement with previous reports, our data indicated higher levels H_2O_2 in sugarcane leaves and led us to speculate that the H_2O_2 levels in sugarcane could modulate *Sc*UGPase-1 activity in response to changes in the redox state of the cell. The inactivation of *Sc*UGPase-1 by redox modification could be explained through S-glutathionylation, as H_2O_2 may inactivate enzymes by oxidizing their thiol groups (66). Under stress conditions, the generation of H_2O_2 can modify the *Sc*UGPase-1 thiol group, resulting in the formation of mixed disulfides between the thiols of *Sc*UGPase-1 and glutathione (GSH). This assumption is supported by evidence demonstrating that crude protein extracts that were prepared from *Arabidopsis* plants and cell cultures were thiolated *in vitro*, and UGPase was one of the proteins that underwent thiolation with oxidized glutathione (GSSG) linked to biotin (67). In this study, it was also demonstrated that by gel filtration chromatography of the oxidized protein it was possible to purify the protein as a dimer. It was previously shown that the accumulation of UDP-Glc decreases UGPase activity by promoting the dimeric association of the protein, instead, the presence of either single or both substrates shifts from UGPase dimers toward monomers, the active form of the enzyme (10). Here, we found that the oligomeric state was also modified in response to changes in the redox conditions, consequently, modulating the enzyme activity. Moreover, the immunoblotting of the proteins of the soluble fraction from the leaves using a barley anti-UGPase antibody detected the monomer and a putative homodimer of the *Sc*UGPase-1 *in vivo*. Although the conditions for the formation of the dimer have not been identified, there is still an evidence of the occurrence of different oligomeric states of the sugarcane protein.

The *Sc*UGPase-1 sequence was compared to other four closely related agronomically important grasses (maize, rice, barley and sorghum) and a model plant, represented by *Arabidopsis thaliana*. All of the sequences that were analyzed by a multiple sequence alignment showed significant identity with *Sc*UGPase-1, and are likely to share details of their tertiary and quaternary structures. UGPase crystallographic structures in the PDB indicated that homologous proteins from *Arabidopsis thaliana* (PDB ID: 1Z90, 2ICX, 2ICY and 2Q4J), *Saccharomyces cerevisiae* (PDB ID: 2IK5) and *Trypanosoma brucei* (PDB ID: 3GUE) contain two molecules in the asymmetric unit (ASU), representing a dimer. This enzyme exists as a mixture of oligomers (monomers, dimers, tetramers, etc.) in solution, with the enzyme in the monomeric state being by far the most catalytically active species (68). According to our small-angle X-ray scattering analysis, the *Sc*UGPase-1 monomeric form has a similar molecular envelope in solution to that of the corresponding monomer of the crystal structure of UGPase from *Arabidopsis thaliana* (PDB ID: 1Z90) (37). A remarkable fact, however, is the unexpected dimer interface that was observed for *Sc*UGPase-1 in solution, which occurs via the C-terminal domain, indicating a configuration that is similar to the end-to-end interaction of different UGPases (human UGPase PDB ID: 3R2W (69), *Saccharomyces cerevisiae* PDB ID: 2IK5 (70), *Arabidopsis thaliana* PDB ID: 1Z90 (37), and *Leishmania major* PDB ID: 2OEG (71)). In addition, as Fig. 10 suggests, the dimer envelope does not correspond to a simple juxtaposition of two identical copies of the monomer envelope, a striking indication that conformational changes most likely occur upon dimerization. Moreover, the static computational model that is shown in Fig. 10 (upper row), although fitting with the SAXS data (which are subject to a low resolution limit), may be composed by domains in different orientations with respect to the *Arabidopsis thaliana* homolog, as indicated by a portion of the envelope that was not perfectly filled by the C-terminus. Altogether,

these results seem to be an indication that *Sc*UGPase-1 undergoes conformational changes upon dimerization that require domain movements involving the C-terminus of the protein. This hypothesis is further supported by a recent study using a deletion of the 8 last amino acids in the C-terminal region of UGPase from barley. As a result, the mutant protein had a higher activity compared to that of the wild-type and was observed only in its monomeric form (11).

Altogether, the results from this study provide insight into the expression profile of the gene that encodes *Sc*UGPase-1 and demonstrate that phosphorylation, membrane association and redox modulation might play roles as regulatory mechanisms of the sucrose metabolic pathway and cell wall biosynthesis.

REFERENCES

1. Waclawovsky, A. J., Sato, P. M., Lembke, C. G., Moore, P. H., and Souza, G. M. (2010) Sugarcane for bioenergy production: an assessment of yield and regulation of sucrose content. *Plant Biotechnol. J.* **8**, 263–76.

2. Matsuoka, S., Ferro, J., and Arruda, P. (2009) The Brazilian experience of sugarcane ethanol industry. *Vitr. Cell. Dev. Biol. - Plant* **45**, 372–381.

3. Arruda, P. (2012) Genetically modified sugarcane for bioenergy generation. *Curr. Opin. Biotechnol.* **23**, 315–22.

4. Botha, F. C., and Black, K. G. (2000) Sucrose phosphate synthase and sucrose synthase activity during maturation of internodal tissue in sugarcane. *Funct. Plant Biol.* **27**, 81.

5. Chen, R., Zhao, X., Shao, Z., Wei, Z., Wang, Y., and L (2007) Rice UDP-glucose pyrophosphorylase1 is essential for pollen callose deposition. *Plant Cell* **19**, 847–861.

6. Amor, Y., Haigler, C. H., Johnson, S., Wainscott, M., and Delmer, D. P. (1995) A membrane-associated form of sucrose synthase and its potential role in synthesis of cellulose and callose in plants. *Proc. Natl. Acad. Sci.* **92**, 9353–9357.

7. Park, J.-I., Ishimizu, T., Suwabe, K., Sudo, K., Masuko, H., Hakozaki, H., Nou, I.-S., Suzuki, G., and Watanabe, M. (2010) UDP-glucose pyrophosphorylase is rate limiting in vegetative and reproductive phases in Arabidopsis thaliana. *Plant cell Physiol.* **51**, 981–996.

8. Kleczkowski, L. A., Geisler, M., Ciereszko, I., and Johansson, H. (2004) UDP-glucose pyrophosphorylase. An old protein with new tricks. *Plant Physiol.* **134**, 912–8.

9. Coleman, H. D., Canam, T., Kang, K.-Y., Ellis, D. D., and Mansfield, S. D. (2007) Over-expression of UDP-glucose pyrophosphorylase in hybrid poplar affects carbon allocation. *J. Exp. Bot.* **58**, 4257–68.

10. Decker, D., Meng, M., Gornicka, A., Hofer, A., Wilczynska, M., and Kleczkowski, L. A. (2012) Substrate kinetics and substrate effects on the quaternary structure of barley UDP-glucose pyrophosphorylase. *Phytochemistry* **79**, 39–45.

11. Meng, M., Fitzek, E., Gajowniczek, A., Wilczynska, M., and Kleczkowski, L. a (2009) Domain-specific determinants of catalysis/substrate binding and the oligomerization status of barley UDP-glucose pyrophosphorylase. *Biochim. Biophys. Acta* **1794**, 1734–42.

12. Alexander, R. D., and Morris, P. C. (2006) A proteomic analysis of 14-3-3 binding proteins from developing barley grains. *Proteomics* **6**, 1886–96.

13. Grose, J. H., Smith, T. L., Sabic, H., and Rutter, J. (2007) Yeast PAS kinase coordinates glucose partitioning in response to metabolic and cell integrity signaling. *EMBO J.* **26**, 4824–30.

14. Varkonyi-Gasic, E., Wu, R., Wood, M., Walton, E. F., and Hellens, R. P. (2007) Protocol: a highly sensitive RT-PCR method for detection and quantification of microRNAs. *Plant Methods* **3**, 12.

15. Papini-Terzi, F. S., Rocha, F. R., Vêncio, R. Z. N., Felix, J. M., Branco, D. S., Waclawovsky, A. J., Del Bem, L. E. V, Lembke, C. G., Costa, M. D. L., Nishiyama, M. Y., Vicentini, R., Vincentz, M. G. A., Ulian, E. C., Menossi, M., and Souza, G. M. (2009) Sugarcane genes associated with sucrose content. *BMC Genomics* **10**, 120.

16. Pabinger, S., Thallinger, G. G., Snajder, R., Eichhorn, H., Rader, R., and Trajanoski, Z. (2009) QPCR: Application for real-time PCR data management and analysis. *BMC Bioinformatics* **10**, 268.

17. Töpfer, R., Matzeit, V., Gronenborn, B., Schell, J., and Steinbiss, H. H. (1987) A set of plant expression vectors for transcriptional and translational fusions. *Nucleic Acids Res.* **15**, 5890.

18. Begcy, K., Mariano, E. D., Gentile, A., Lembke, C. G., Zingaretti, S. M., Souza, G. M., and Menossi, M. (2012) A novel stress-induced sugarcane gene confers tolerance to drought, salt and oxidative stress in transgenic tobacco plants. *PLoS One* **7**, e44697.

19. Fusari, C., Demonte, A. M., Figueroa, C. M., Aleanzi, M., and Iglesias, A. A. (2006) A colorimetric method for the assay of ADP-glucose pyrophosphorylase. *Anal. Biochem.* **352**, 145–7.

20. Kellermann, G., Vicentin, F., Tamura, E., Rocha, M., Tolentino, H., Barbosa, A., Craievich, A., and Torriani, I. (1997) The Small-Angle X-ray Scattering Beamline of the Brazilian Synchrotron Light Laboratory. *J. Appl. Crystallogr.* **30**, 880–883.

21. Orthaber, D., Bergmann, A., and Glatter, O. (2000) SAXS experiments on absolute scale with Kratky systems using water as a secondary standard. *J. Appl. Crystallogr.* **33**, 218–225.

22. Mylonas, E., and Svergun, D. I. (2007) Accuracy of molecular mass determination of proteins in solution by small-angle X-ray scattering. *J. Appl. Crystallogr.* **40**, s245–s249.

23. Hammersley, A. P., Svensson, S. O., Hanfland, M., Fitch, A. N., and Hausermann, D. (1996) Two-dimensional detector software: From real detector to idealised image or two-theta scan. *High Press. Res.* **14**, 235–248.

24. Petoukhov, M. V., Franke, D., Shkumatov, A. V., Tria, G., Kikhney, A. G., Gajda, M., Gorba, C., Mertens, H. D. T., Konarev, P. V., and Svergun, D. I. (2012) New developments in the ATSAS program package for small-angle scattering data analysis. *J. Appl. Crystallogr.* **45**, 342–350.

25. Mertens, H. D. T., and Svergun, D. I. (2010) Structural characterization of proteins and complexes using small-angle X-ray solution scattering. *J. Struct. Biol.* **172**, 128–41.

26. Svergun, D. I. (1992) Determination of the regularization parameter in indirect-transform methods using perceptual criteria. *J. Appl. Crystallogr.* **25**, 495–503.

27. Rambo, R. P., and Tainer, J. A. (2011) Characterizing flexible and intrinsically unstructured biological macromolecules by SAS using the Porod-Debye law. *Biopolymers* **95**, 559–71.

28. Doniach, S. (2001) Changes in Biomolecular Conformation Seen by Small Angle X-ray Scattering. *Chem. Rev.* **101**, 1763–1778.

29. Semisotnov, G. V., Kihara, H., Kotova, N. V., Kimura, K., Amemiya, Y., Wakabayashi, K., Serdyuk, I. N., Timchenko, A. A., Chiba, K., Nikaido, K., Ikura, T., and Kuwajima, K. (1996) Protein Globularization During Folding. A Study by Synchrotron Small-angle X-ray Scattering. *J. Mol. Biol.* **262**, 559–574.

30. Fischer, H., de Oliveira Neto, M., Napolitano, H. B., Polikarpov, I., and Craievich, A. F. (2009) Determination of the molecular weight of proteins in solution from a single small-angle X-ray scattering measurement on a relative scale. *J. Appl. Crystallogr.* **43**, 101–109.

31. Svergun, D. I., Petoukhov, M. V, and Koch, M. H. (2001) Determination of domain structure of proteins from X-ray solution scattering. *Biophys. J.* **80**, 2946–53.

32. Franke, D., and Svergun, D. I. (2009) DAMMIF , a program for rapid ab-initio shape determination in small-angle scattering. *J. Appl. Crystallogr.* **42**, 342–346.

33. Volkov, V. V., and Svergun, D. I. (2003) Uniqueness of ab initio shape determination in small-angle scattering. *J. Appl. Crystallogr.* **36**, 860–864.

34. Roy, A., Kucukural, A., and Zhang, Y. (2010) I-TASSER: a unified platform for automated protein structure and function prediction. *Nat. Protoc.* **5**, 725–38.

35. dos Reis, M. A., Aparicio, R., and Zhang, Y. (2011) Improving Protein Template Recognition by Using Small-Angle X-Ray Scattering Profiles. *Biophys. J.* **101**, 2770–2781.

36. Svergun, D., Barberato, C., and Koch, M. H. J. (1995) CRYSOL - a Program to Evaluate X-ray Solution Scattering of Biological Macromolecules from Atomic Coordinates. *J. Appl. Crystallogr.* **28**, 768–773.

37. McCoy, J. G., Bitto, E., Bingman, C. A., Wesenberg, G. E., Bannen, R. M., Kondrashov, D. A., and Phillips, G. N. (2007) Structure and dynamics of UDP-glucose pyrophosphorylase from Arabidopsis thaliana with bound UDP-glucose and UTP. *J. Mol. Biol.* **366**, 830–41.

38. Kozin, M. B., and Svergun, D. I. (2001) Automated matching of high- and low-resolution structural models. *J. Appl. Crystallogr.* **34**, 33–41.

39. Sayle, R. A., and Milner-White, E. J. (1995) *RASMOL: biomolecular graphics for all*.

40. Zrenner, R., Willmitzer, L., and Sonnewald, U. (1993) Analysis of the expression of potato uridinediphosphate-glucose pyrophosphorylase and its inhibition by antisense RNA. *Planta* **190**, 247–52.

41. Gupta, S. K., Sowokinos, J. R., and Hahn, I.-S. (2008) Regulation of UDP-glucose pyrophosphorylase isozyme UGP5 associated with cold-sweetening resistance in potatoes. *J. Plant Physiol.* **165**, 679–90.

42. Becker, M., Vincent, C., and Grant Reid, J. S. (1995) Biosynthesis of (1,3)(1,4)-?-glucan and (1,3)-?-glucan in barley (Hordeum vulgare L.). *Planta* **195**, 331–338.

43. Kolodziejski, P. J., Rashid, M. B., and Eissa, N. T. (2003) Intracellular formation of "undisruptable" dimers of inducible nitric oxide synthase. *Proc. Natl. Acad. Sci. U. S. A.* **100**, 14263–8.

44. Salahpour, A., Bonin, H., Bhalla, S., Petäjä-Repo, U., and Bouvier, M. (2003) Biochemical Characterization of β2-Adrenergic Receptor Dimers and Oligomers. *Biol. Chem.* **384**, 117–123.

45. Koo, J. H., Gill, S., Pannell, L. K., Menco, B. P. M., Margolis, J. W., and Margolis, F. L. (2004) The interaction of Bex and OMP reveals a dimer of OMP with a short half-life. *J. Neurochem.* **90**, 102–16.

46. Manning, M., and Colón, W. (2004) Structural basis of protein kinetic stability: resistance to sodium dodecyl sulfate suggests a central role for rigidity and a bias toward beta-sheet structure. *Biochemistry* **43**, 11248–54.

47. Martínez, L. I., Piattoni, C. V, Garay, S. A., Rodrígues, D. E., Guerrero, S. A., and Iglesias, A. A. (2011) Redox regulation of UDP-glucose pyrophosphorylase from Entamoeba histolytica. *Biochimie* **93**, 260–8.

48. Cheeseman, J. M. (2006) Hydrogen peroxide concentrations in leaves under natural conditions. *J. Exp. Bot.* **57**, 2435–44.

49. Meng, M., Wilczynska, M., and Kleczkowski, L. A. (2008) Molecular and kinetic characterization of two UDP-glucose pyrophosphorylases, products of distinct genes, from Arabidopsis. *Biochim. Biophys. Acta* **1784**, 967–72.

50. Pua, E.-C., Lim, S. S.-W., Liu, P., and Liu, J.-Z. (2000) Expression of a UDPglucose pyrophosphorylase cDNA during fruit ripening of banana (Musa acuminata). *Funct. Plant Biol.* **27**, 1151–1159.

51. Ciereszko, I., Johansson, H., and Kleczkowski, L. A. (2001) Sucrose and light regulation of a cold-inducible UDP-glucose pyrophosphorylase gene via a hexokinase-independent and abscisic acid-insensitive pathway in Arabidopsis. *Biochem. J.* **354**, 67–72.

52. Ciereszko, I., Johansson, H., Hurry, V., and Kleczkowski, L. A. (2001) Phosphate status affects the gene expression, protein content and enzymatic activity of UDP-glucose pyrophosphorylase in wild-type and pho mutants of Arabidopsis. *Planta* **212**, 598–605.

53. Moore, P. (1995) Temporal and Spatial Regulation of Sucrose Accumulation in the Sugarcane Stem. *Aust. J. Plant Physiol.* **22**, 661.

54. Zhu, Y. J., Komor, E., and Moore, P. H. (1997) Sucrose Accumulation in the Sugarcane Stem Is Regulated by the Difference between the Activities of Soluble Acid Invertase and Sucrose Phosphate Synthase. *Plant Physiol.* **115**, 609–616.

55. Ciereszko, I., Johansson, H., and Kleczkowski, L. A. (2005) Interactive effects of phosphate deficiency, sucrose and light/dark conditions on gene expression of UDP-glucose pyrophosphorylase in Arabidopsis. *J. Plant Physiol.* **162**, 343–53.

56. Meng, M., Geisler, M., Johansson, H., Mellerowicz, E. J., Karpinski, S., and Kleczkowski, L. A. (2007) Differential tissue/organ-dependent expression of two sucrose- and cold-responsive genes for UDP-glucose pyrophosphorylase in Populus. *Gene* **389**, 186–95.

57. Mikami, S., Hori, H., and Mitsui, T. (2001) Separation of distinct compartments of rice Golgi complex by sucrose density gradient centrifugation. *Plant Sci.* **161**, 665–675.

58. Kleczkowski, L., Kunz, S., and Wilczynska, M. (2010) Mechanisms of UDP-Glucose Synthesis in Plants. *CRC. Crit. Rev. Plant Sci.* **29**, 191–203.

59. Winter, H., and Huber, S. C. (2000) Regulation of Sucrose Metabolism in Higher Plants: Localization and Regulation of Activity of Key Enzymes. *Crit. Rev. Biochem. Mol. Biol.* **35**, 253–289.

60. Rutter, J., Probst, B. L., and McKnight, S. L. (2002) Coordinate Regulation of Sugar Flux and Translation by PAS Kinase. *Cell* **111**, 17–28.

61. Toroser, D., Athwal, G. S., and Huber, S. C. (1998) Site-specific regulatory interaction between spinach leaf sucrose-phosphate synthase and 14-3-3 proteins. *FEBS Lett.* **435**, 110–114.

62. Stitt, M., Wilke, I., Feil, R., and Heldt, H. W. (1988) Coarse control of sucrose-phosphate synthase in leaves: Alterations of the kinetic properties in response to the rate of photosynthesis and the accumulation of sucrose. *Planta* **174**, 217–30.

63. Barratt, D. H. P., Derbyshire, P., Findlay, K., Pike, M., Wellner, N., Lunn, J., Feil, R., Simpson, C., Maule, A. J., and Smith, A. M. (2009) Normal growth of Arabidopsis requires cytosolic invertase but not sucrose synthase. *Proc. Natl. Acad. Sci. U. S. A.* **106**, 13124–9.

64. Yan, S., Tang, Z., Su, W., and Sun, W. (2005) Proteomic analysis of salt stress-responsive proteins in rice root. *Proteomics* **5**, 235–44.

65. Van den Ende, W., and Valluru, R. (2009) Sucrose, sucrosyl oligosaccharides, and oxidative stress: scavenging and salvaging? *J. Exp. Bot.* **60**, 9–18.

66. Gill, S. S., and Tuteja, N. (2010) Reactive oxygen species and antioxidant machinery in abiotic stress tolerance in crop plants. *Plant Physiol. Biochem.* **48**, 909–30.

67. Dixon, D. P., Skipsey, M., Grundy, N. M., and Edwards, R. (2005) Stress-induced protein S-glutathionylation in Arabidopsis. *Plant Physiol.* **138**, 2233–44.

68. Martz, F., Wilczynska, M., and Kleczkowski, L. a (2002) Oligomerization status, with the monomer as active species, defines catalytic efficiency of UDP-glucose pyrophosphorylase. *Biochem. J.* **367**, 295–300.

69. Yu, Q., and Zheng, X. (2012) The crystal structure of human UDP-glucose pyrophosphorylase reveals a latch effect that influences enzymatic activity. *Biochem. J.* **442**, 283–91.

70. Roeben, A., Plitzko, J. M., Körner, R., Böttcher, U. M. K., Siegers, K., Hayer-Hartl, M., and Bracher, A. (2006) Structural basis for subunit assembly in UDP-glucose pyrophosphorylase from Saccharomyces cerevisiae. *J. Mol. Biol.* **364**, 551–60.

71. Steiner, T., Lamerz, A.-C., Hess, P., Breithaupt, C., Krapp, S., Bourenkov, G., Huber, R., Gerardy-Schahn, R., and Jacob, U. (2007) Open and closed structures of the UDP-glucose pyrophosphorylase from Leishmania major. *J. Biol. Chem.* **282**, 13003–10.

Acknowledgements- The authors wish to thank Prof. Dr. Leszek A. Kleczkowski for providing the barley anti-UGPase antibody. In addition, we are grateful for the access to equipment and assistance provided by the National Institute of Science and Technology on Photonics Applied to Cell Biology (INFABIC) at the University of Campinas (UNICAMP). We gratefully acknowledge beamline time that was provided by the Laboratório Nacional de Luz Síncrotron (LNLS, Campinas, Brazil). The authors are also very grateful to Dr. Mateus B. Cardoso (LNLS) for helpful discussions on the SAXS experiments and data processing.

Footnotes

***** This work was supported by the Fundação de Amparo à Pesquisa do Estado de São Paulo (FAPESP grant 2008/06767-3) and Coordenação de Aperfeiçoamento de Pessoal de Nível Superior (CAPES grant BEX 0095/10-9). C.V.P. was supported by CONICET and NSF. R.A. is recipient of a research fellowship from CNPq.

[1]To whom correspondence should be addressed: Marcelo Menossi, Departmento de Genética, Evolução e Bioagentes, Instituto de Biologia, Universidade Estadual de Campinas, Rua Monteiro Lobato, 255, Campinas, SP, Brazil, tel.: +55 (19) 3521-6236; +55 (19) 3521-6241; E-mail: menossi@lgf.ib.unicamp.br

The abbreviations used are as follows: ASU, asymmetric units; *At*UGPase, *Arabidopsis thaliana* UDP-glucose pyrophosphorylase; BSA, bovine serum albumin; cDNA, complementary DNA; DTT, dithiothreitol; EDTA, ethylenediaminetetraacetate; Glc-1-P, glucose-1-phosphate; GFP, green fluorescent protein; IMAC, immobilized metal ion affinity chromatography; IPTG, isopropyl β-D-1-thiogalactopyranoside; LB, Luria Bertani; Ni-NTA, nickel nitrilotriacetic acid; PBS, phosphate buffered saline; PBST, phosphate buffered saline with Tween-20; PDB, protein data bank; PMSF, phenylmethanesulfonylfluoride; P(r), pair-distance distribution function; Rg, radius of gyration; RT-qPCR, reverse transcription quantitative polymerase chain reaction; SAXS, small-angle X-ray scattering; *Sc*UGPase-1, *Saccharum spp* UDP-glucose pyrophosphorylase; SDS-PAGE, sodium dodecyl sulfate polyacrylamide gel electrophoresis; SPS, sucrose phosphate synthase; SuSy, sucrose synthase; UGPase, UDP-glucose pyrophosphorylase; UTP, uridine 5'-triphosphate.

Figure Legends

Table 1. Specific primers that were used for the experiments.

Table 2. Kinetic parameters of the recombinant *Sc*UGPase-1.

Figure 1. Relative expression of *ScUGPase-1* as determined by RT-qPCR from two sugarcane cultivars contrasting in sucrose content. (A) Real time PCR results for the sugarcane cultivar RB855156 with a high sucrose content. (B) Real time PCR results for the sugarcane cultivar RB 935744 with a low sucrose content. The reactions were performed in triplicate. * indicates $p<0.05$.

Figure 2. Immunoblotting analysis of the membrane and soluble fraction of *Sc*UGPase-1 in the internodes and leaves. Immunoblot of the internodes (A) and leaves (B) using an anti-*Hv*UGPase antibody. The numbers indicate the proteins of the microsomal fraction (1), the proteins of the soluble fraction (2) and the *Sc*UGPase-1 recombinant protein (3). M, molecular weight standard.

Figure 3. Multiple sequence alignment of UGPases from different plant species. Accession number KF278717 (*Saccharum spp* UGPase), accession number ACG32096 (*Zea mays* UGPase), accession number ACA50487 (*Oryza sativa* UGPase), accession number CAA62689 (*Hordeum vulgare* UGPase), accession number XP_002453185 (*Sorghum bicolor* UGPase) and accession number P19595 (*Arabidopsis thaliana* UGPase). The blue triangle indicates the serine that is predicted to be phosphorylated at the 14-3-3 binding site.

Figure 4. Phosphorylation analysis of the membrane and soluble fraction of *Sc*UGPase-1 in the internodes and leaves. Immunoblot of the internodes (A) and leaves (B) using an anti-pS419 antibody. The numbers indicate the proteins of the microsomal fraction (1), the proteins of the soluble fraction (2) and the *Sc*UGPase-1 recombinant protein (3). M, molecular weight standard.

Figure 5. Subcellular localization of GFP-*Sc*UGPase-1. **(**A) pRT104::*Sc*UGPase-1-GFP construction map. (B) Confocal microscopy of an onion epidermis cell expressing the GFP-*Sc*UGPase-1. The bars represent 100 µm.

Figure 6. SDS-PAGE of the recombinant *Sc*UGPase-1. (1) The 6× his-tagged *Sc*UGPase-1 and (2) recombinant *Sc*UGPase-1 after cleavage with the rTEV protease. M, molecular weight standard. After electrophoresis, the gel was stained with *Coomassie blue*.

Figure 7. Saturation curves for the recombinant *Sc*UGPase-1. (A) Glc-1-P concentration ranging from 0 to 2.5 mM. (B) UTP concentration ranging from 0 to 3.5 mM. (C) Mg^{2+} concentration ranging from 0 to 20 mM. When each substrate was analyzed, the other two substrates were maintained at a fixed saturation concentration.

Figure 8. Redox regulation of the recombinant *Sc*UGPase-1 activity. (A) Inactivation of *Sc*UGPase-1 by different concentrations of H_2O_2. (B) Effect of the reducing agent DTT on oxidized *Sc*UGPase-1.

Figure 9. SAXS analysis of the *Sc*UGPase-1 constructs in solution. (A) Final monomer scattering curve (open squares) with an inset showing the linear fitting in the Guinier region. The solid line corresponds to the fitting of the theoretical curve that was calculated for the *Sc*UGPase-1 monomer that was obtained by computational methods. A χ value of 2.55 was obtained with CRYSOL (36) up to a q_{max} = 0.25, as shown in the plot. Values as low as 1.44 were obtained, limiting the range to 0.20 $Å^{-1}$and indicating, a correspondence of the gross low resolution features of the scattering particle in solution and the monomer rigid model. (B) Solution scattering profile (open circles) of the *Sc*UGPase-1 dimer in the q range that

was limited after data processing. The inset shows the linear fitting that was obtained from the Guinier analysis. The solid line corresponds to the fitting of the theoretical curve as calculated for the computational dimer model in the same range that was automatically refined by PRIMUS/AUTOGNOM (24) during the indirect Fourier transform procedure. The discrepancy between the experimental data and the theoretical curve was calculated by CRYSOL, resulting in a χ value of 1.45. (C) Kratky plot that was derived from the experimental curves that were normalized for I(0) = 1 for proper visualization. After buffer scattering subtraction, a few negative intensity points were obtained for the dimer curve at higher q values due to the very low sample concentration. The plot is limited to the region $Iq^2 > 0$. (D) Distance distribution function as calculated from the experimental curve that was used for the *ab initio* envelope reconstruction. The monomer P(r) (open squares) exhibits a nearly centered peak, indicating a globular scattering particle. For the second sample, a typical profile with two clearly distinct maxima indicates the presence of a dimer in solution, as anticipated by the molecular mass estimates; the higher peak to the left of the center of the range indicates that the dimer exhibits a prolate shape.

Figure 10. PyMOL surface representations of the monomer (upper row) and dimer (bottom row) as recovered from the experimental SAXS data that were superposed onto the respective computational models, represented as a cartoon drawing and viewed nearly along the point-group P2 dimer symmetry. The solvent layer sparsely distributed over the protein surface, as calculated by GASBOR (31), is shown as spheres. For the dimer, each monomer chain is shown in different hues of yellow; the N-terminus containing the 6× his-tag, disordered in solution as indicated by the computational analysis, was omitted for clarity. The scale and perspectives are the same in both rows. The middle and right columns are rotated clockwise by 90º around the y- and x-axes, respectively. The figures were prepared with PyMOL and edited using GIMP (http://www.gimp.org) under Slackware Linux (http://www.slackware.com).

Table 1

Primer name	Sequence (5'-3')	Nt	Tm (°C)
*Sc*UGPase-1_Fw	CAC CGC CGC CGC TGC C	16	59
*Sc*UGPase-1_Rv	TTA AAG ATC CTC AGG GCC A	19	53
pRT104-*Sc*UGPase_Fw	CAT GGA GGC CGA ATT CAT GGC CGC CGC TG	29	68
pRT104-*Sc*UGPase_Rv	GCA GGT CGA CGG ATC CAA GAT CCT CAG GGC CA	32	65
RT-*Sc*UGPase_Fw	TCC AGC TAA CCC TTC GAT TGA G	22	56
RT-*Sc*UGPase_Rv	GAG CAA GGA AAT TGG CAA CCT	21	56.2
PUB-Fw	CCG GTC CTT TAA ACC AAC TCA GT	23	57
PUB-Rv	CCC TCT GGT GTA CCT CCA TTT G	22	57.3

Table 2

Substrate	K_m **(mM)**	k_{cat} **(s^{-1})**	k_{cat}/K_m **($s^{-1}\cdot mM^{-1}$)**
Synthesis direction			
Glc-1-P	0.20 ± 0.01		9×10^{8}
UTP	0.16 ± 0.01	1.8×10^{8}	1.1×10^{9}
Mg^{2+}	1.26 ± 0.06		

Figure 1

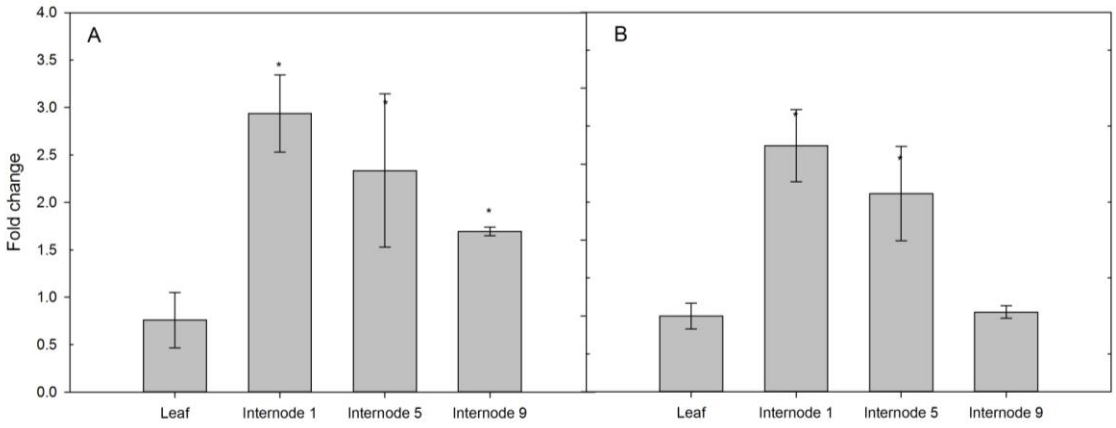

Figure 2

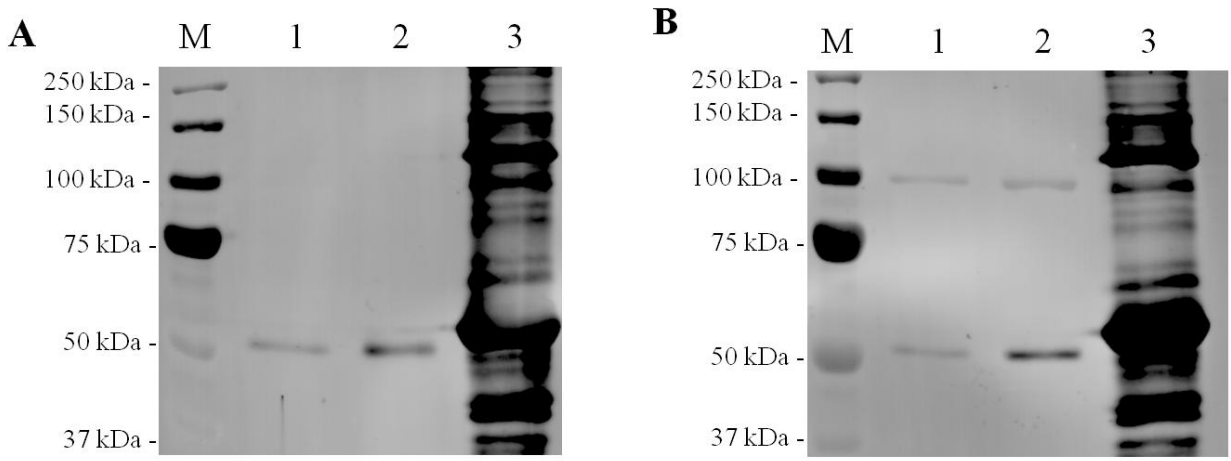

Figure 3

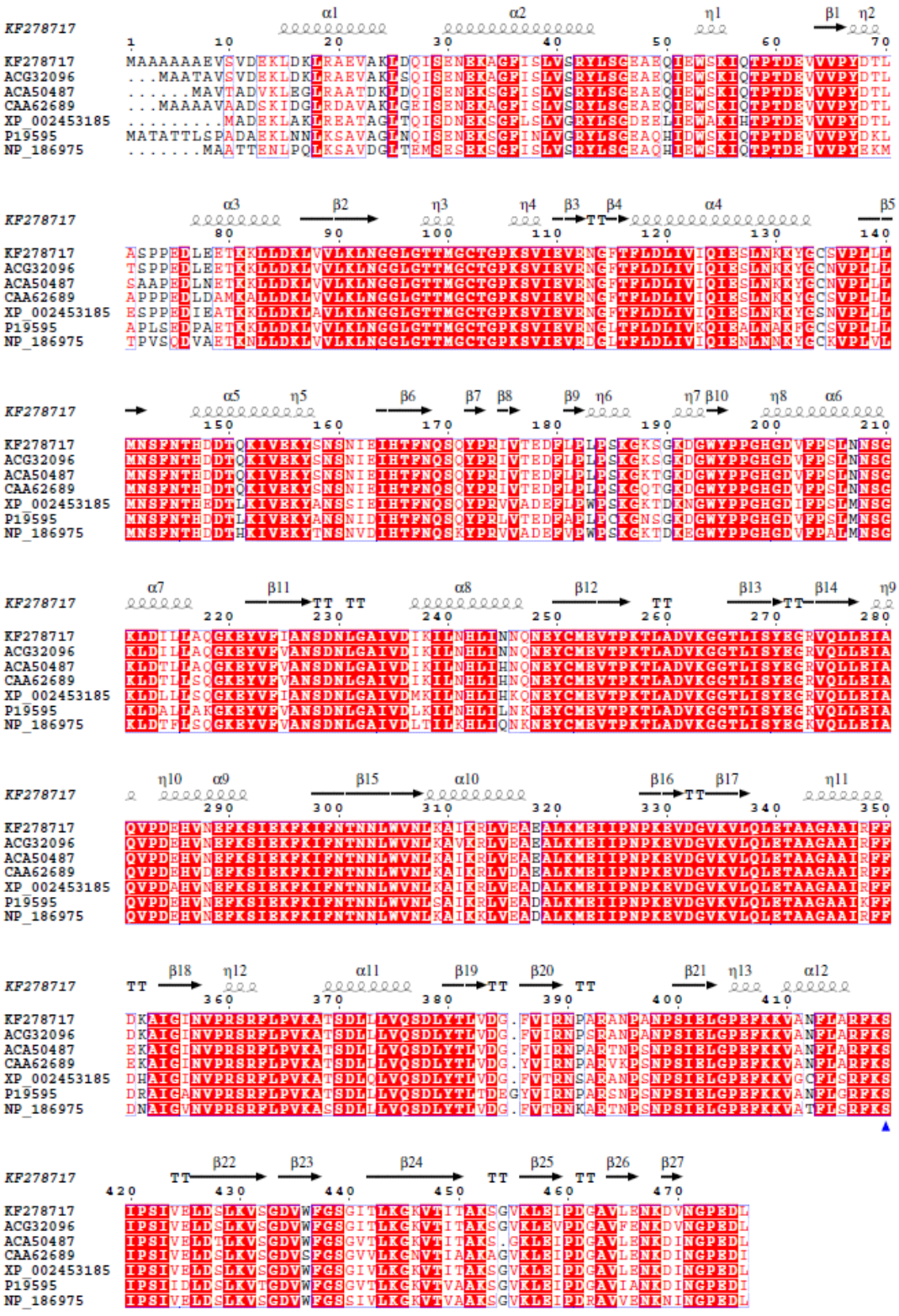

Figure 4

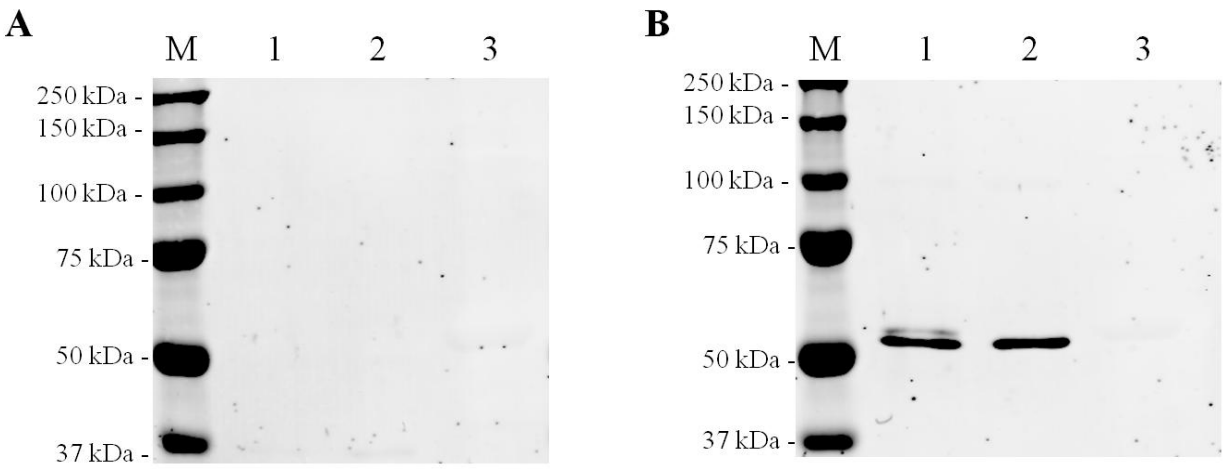

Figure 5

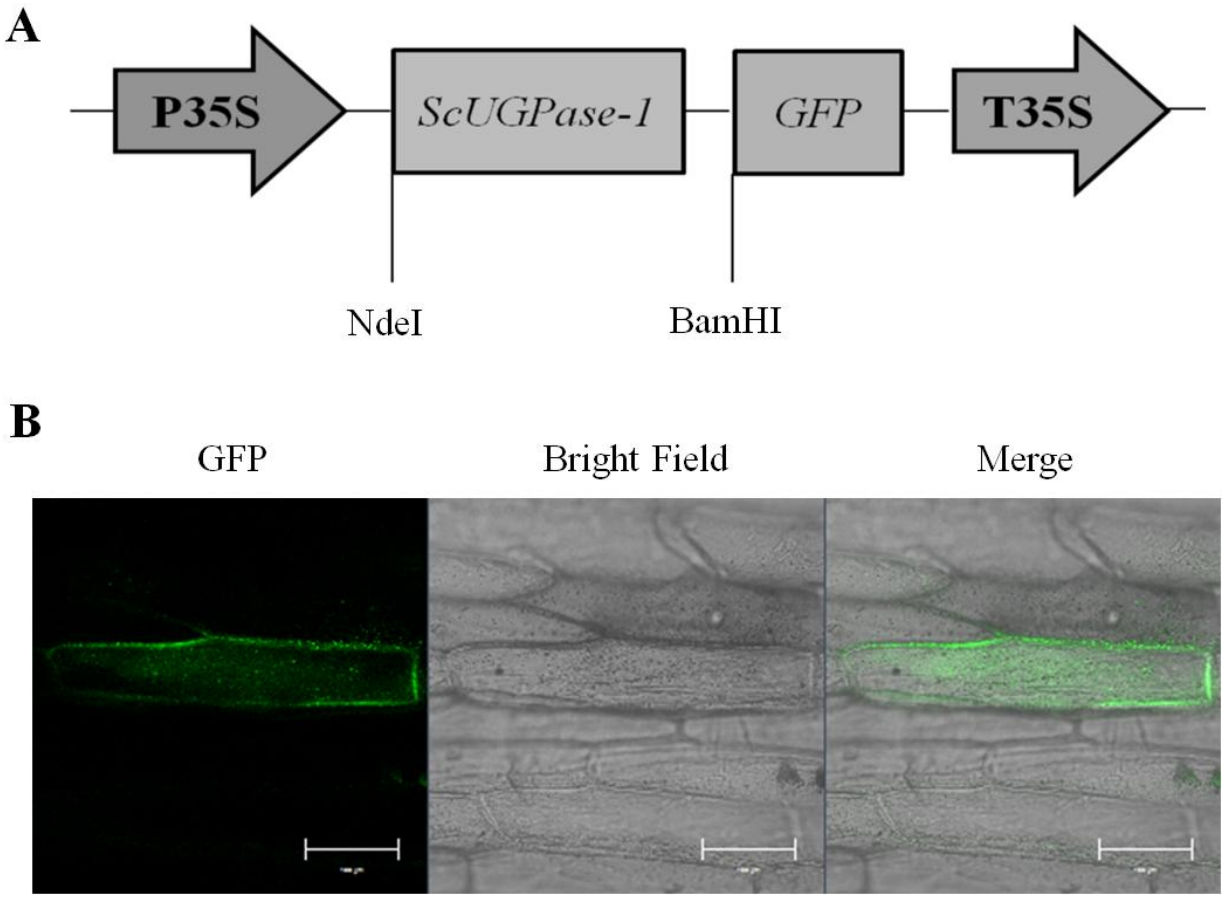

Figure 6

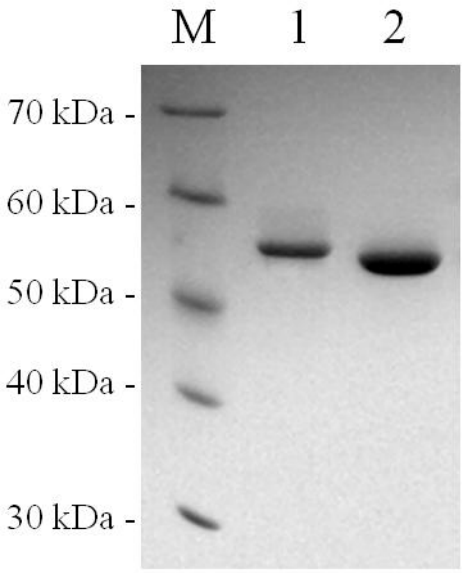

Figure 7

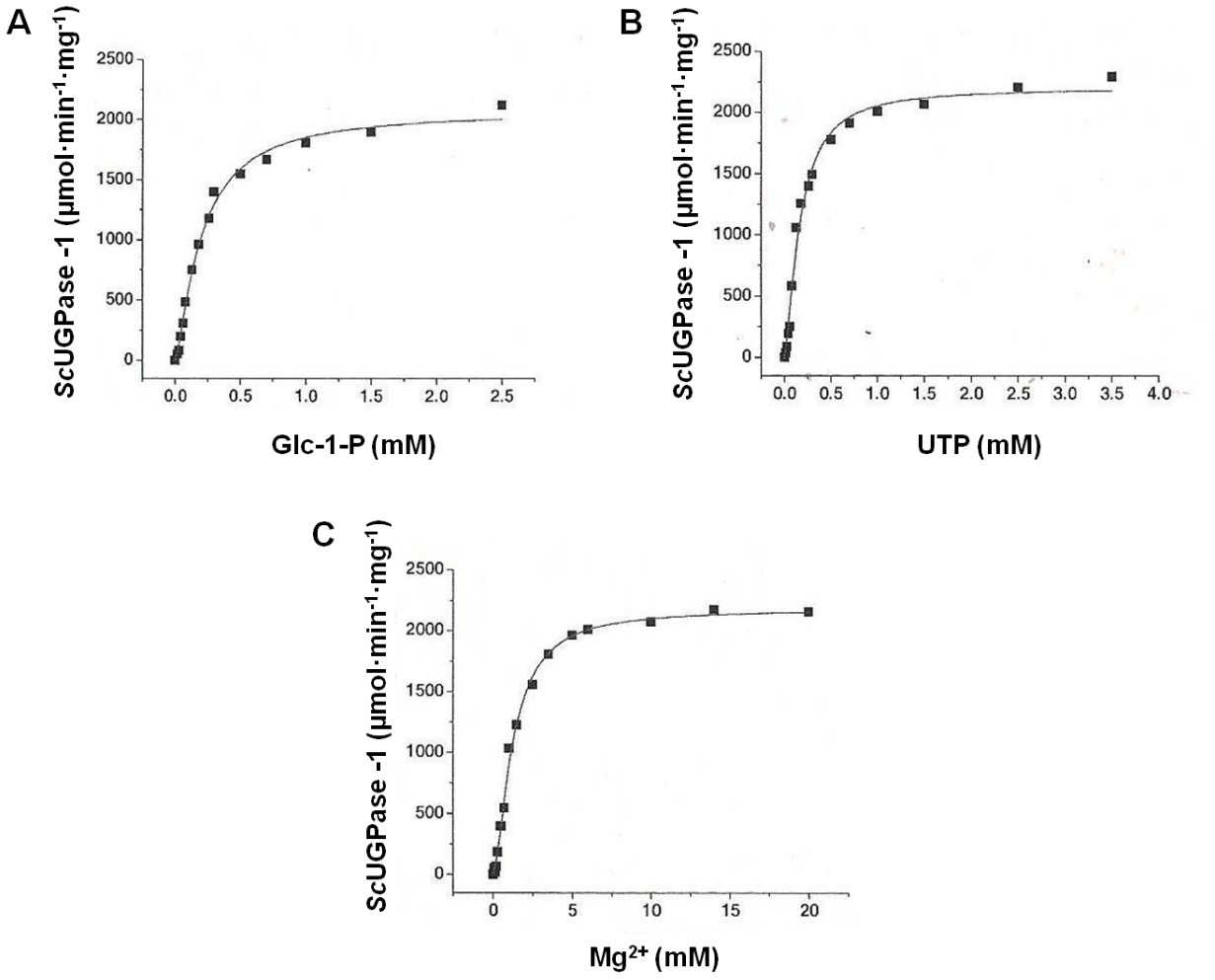

Figure 8

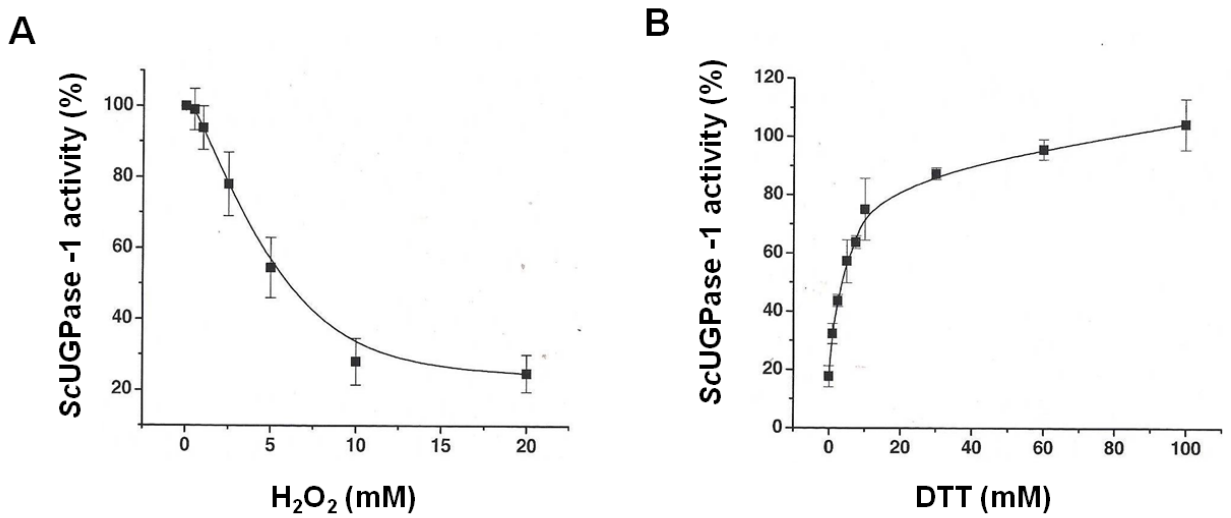

Figure 9

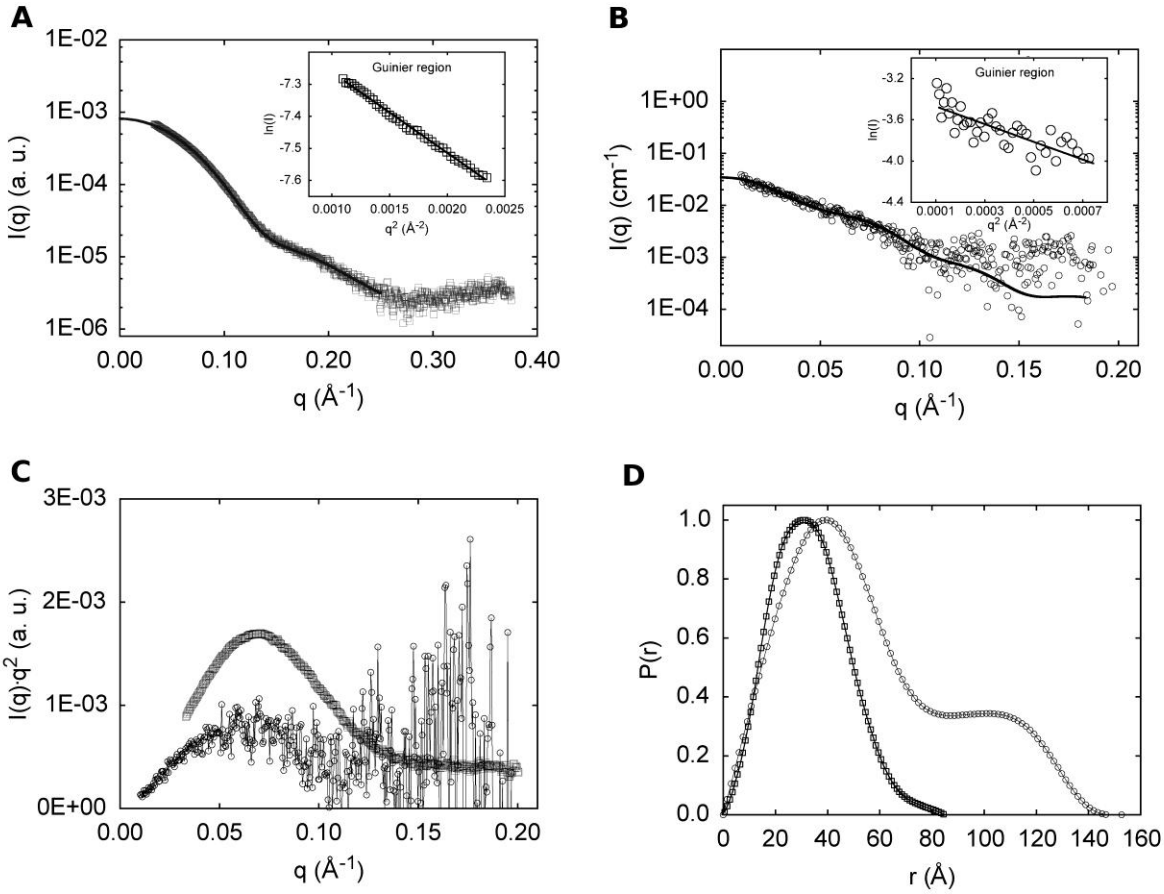

Figure 10